Astron. Astrophys. 319, 547–560 (1997)

ASTRONOMY
AND
ASTROPHYSICS

Protostellar binary fragmentation: a comparison of results from two distinct second-order hydrodynamic codes

Leonardo Di G. Sigalotti[1] **and Jaime Klapp**[2]

[1] International School for Advanced Studies, SISSA, Via Beirut 2-4, I-34013 Trieste, Italy
[2] Instituto Nacional de Investigaciones Nucleares, ININ, Apartado Postal 18-1027, Mexico 11801 DF

Received 4 March 1996 / Accepted 2 July 1996

Abstract. A new second-order Eulerian code is compared with a version of the TREESPH code formulated by Hernquist & Katz (1989) for the standard isothermal collapse test. The results indicate that both codes produce a very similar evolution ending with the formation of a protostellar binary system. Contrary to previous first-order calculations, the binary forms by direct fragmentation, i.e., without the occurrence of an intermediate bar configuration. A similar trend was also found in recent second-order Eulerian calculations (Myhill & Boss 1993), suggesting that it is a result of the decreased numerical diffusion associated with the new second-order schemes. The results have also implications on the differences between the finite difference methods and the particle method SPH, raised by Monaghan & Lattanzio (1986) for this problem. In particular, the Eulerian calculation does not result in a run-away collapse of the fragments, and as found in the TREESPH evolution, they also show a clear tendency to get closer together. In agreement with previous SPH calculations (Monaghan & Lattanzio 1986), the results of the long term evolution with code TREESPH show that the gravitational interaction between the two fragments may become important, and eventually induce the binary to coalesce. However, most recent SPH calculations (Bate, Bonnell & Price 1995) indicate that the two fragments, after having reached a minimum separation distance, do not merge but continue to orbit each other.

Key words: hydrodynamics – methods: numerical – stars: formation

1. Introduction

The basic motivation for this paper is the comparison of two new and entirely independent three-dimensional (3D), hydrodynamic computer codes for the calculation of self-gravitating flows with rotation. The codes are based on completely different numerical methods and are second-order accurate in space and time. One code solves the equations of Eulerian hydrodynamics using specialized finite difference (FD) methods on a radially moving, spherical coordinate grid. This code is an improved extension of a previously implemented second-order FD scheme (Sigalotti 1993). The other code is a gridless one based on the TREESPH method, i.e., it uses a smoothed particle hydrodynamic (SPH) approach coupled with the hierarchical tree algorithm of Hernquist (1987) for the calculation of the gravitational forces.

In order to see how the results from both schemes compare, we have considered as a test model calculation, the isothermal collapse and fragmentation of a protostellar gas cloud with initial rotation. The set of initial conditions used corresponds to that originally advanced by Boss & Bodenheimer (1979), and thereafter known as the "standard test case" for 3D protostellar collapse codes. This choice of the initial conditions is justified by the following two reasons. First, they allow for a direct comparison of the new schemes for a problem involving the growth of density perturbations in a collapsing medium with simplified thermodynamics. Second, they allow us to compare our results with those from other SPH (Monaghan & Lattanzio 1986, hereafter ML; Bate, Bonnell & Price 1995) and second-order FD calculations (Myhill & Boss 1993, hereafter MB). In particular, MB compared a Cartesian coordinate scheme with a spherical coordinate-based code (Boss & Myhill 1992) for this test problem.

The results for this test with both of our codes show that the outcome of the collapse is the formation of a protostellar binary system in agreement with ML and MB calculations. However, an important aspect of the present results is that the intermediate features of the collapse, as followed by the two new codes, are very similar. This has direct implications on the concerns raised by ML over basic differences between the FD and the SPH methods for this test problem. We find that up to the time the calculations could be compared, the variation of the maximum density with time is in good agreement for both methods, with the general trends of the evolution being rather independent of resolution. A clear tendency for the growing binary fragments to fall towards each other during the evolution is also observed in

both calculations. This aspect of the solution was first demonstrated by Gingold & Monaghan (1981) and then reproduced independently by ML and Bate et al. (1995).

A further important question concerning the standard test case is whether binary fragmentation occurs directly from the continual growth of the initial density perturbation or through the formation of an intermediate bar configuration. In previous first-order FD calculations, the cloud collapsed to form a central bar configuration which then fragmented into a binary system. On the contrary, the second-order calculations of MB showed that the cloud can fragment directly without the formation of a well-defined central bar. With their spherical coordinate code, however, the disappearance of the intermediate bar was observed only when the resolution near the equatorial plane was increased further. So they concluded that for spherical coordinate-based codes having increasing equatorial resolution - in order to solve adequately the rotationally flattened disk that forms from collapse - would be as important as having decreased numerical diffusion. In the TREESPH calculations, binary fragmentation occurs all the way without the formation of an intermediate bar configuration. This result, however, is not surprising because of the relative non-diffusiveness of the TREESPH method, and because of its gridless nature which makes the calculation free of mesh-related limitations on the dynamic range in spatial resolution. Unexpectedly, the FD code with much coarser resolution near the equatorial plane than that used in MB, produced an intermediate evolution very similar to that calculated with the TREESPH code. We conclude that the disappearance of the intermediate bar is merely a consequence of the smaller diffusive truncation errors associated with the new spherical FD code, and that any second-order FD scheme would be able to reproduce this feature without the need of enhanced equatorial resolution. This is a quite desirable property of the new FD methods since starting the calculations either with a stretched grid or with a finer mesh everywhere will inevitably increase the CPU demands required for spherical coordinate-based codes.

The comparison of the results from both schemes is also extended to the evaluation of the fragment properties. A method which improves on the accuracy of the rotational properties is given. In Sect. 2 we summarize the initial conditions and give a brief description of the numerical methods. The results of this comparison test case are discussed in Sect. 3. Finally, Sect. 4 contains the conclusions.

2. Initial model and numerical methods

2.1. The initial model

For our test model calculations we have chosen an idealized set of initial conditions corresponding to the standard isothermal test case (Boss & Bodenheimer 1979). The initial model consists of a $1M_{\odot}$, uniform density ($\rho_0 = 1.44 \times 10^{-17}$ g cm^{-3}), uniformly rotating ($\omega_0 = 1.56 \times 10^{-12}$ s^{-1}) sphere of radius $R = 3.20 \times 10^{16}$ cm, composed of pure molecular hydrogen at a temperature of 10 K. An azimuthally varying perturbation of the form

$$\rho = \rho_0 \left[1 + a \cos(m\phi)\right] \quad , \tag{1}$$

with mode $m = 2$ and amplitude $a = 0.5$, is added to the background uniform density distribution. During the evolution, the cloud is assumed to remain isothermal ($\gamma = 1$) at a constant temperature equal to the initial value of 10 K. With these initial parameters, the ratios of thermal and rotational to the cloud's self-gravitational energy are, respectively, $\alpha = 0.25$ and $\beta = 0.20$.

Previous calculations of the standard test case using first-order accurate FD (Boss & Bodenheimer 1979; Bodenheimer & Boss 1981; de Felice & Sigalotti 1992), SPH (Gingold & Monaghan 1981; ML; Bate et al. 1995) and second-order accurate FD codes (MB; Burkert & Bodenheimer 1993) have shown a fairly good agreement that the outcome of the first evolution is the formation of a binary system. Nevertheless, basic differences between the FD and the SPH methods (ML) still remain to be clarified. In order to address this point we have rerun the standard test model using two new distinct codes. In the sequel we shall refer to them as code FD and code TREESPH.

2.2. Code FD

Code FD is a fully 3D radiation hydrodynamic scheme written in Eulerian spherical coordinates (r, θ, ϕ). It is a descendant of a previously implemented FD code (Sigalotti 1993). For the purposes of this paper, we have used a simplified version of the code, which solves the equations of continuity and motion in conservation-law form for a compressible, inviscid, non-magnetic fluid, coupled with the Poisson equation for the gravitational potential. This set of equations is closed by specifying a pressure relation of the form $p \propto \rho$, where ρ is the mass-density. The above equations are solved using FD methods on a radially moving spherical grid along with a multi-step solution procedure for the hydrodynamic equations in which the source and the convective terms are evaluated in separate sub-steps. The time integration of the hydrodynamic equations is made explicitly and is optionally first- or second-order accurate. Temporal second-order accuracy is achieved by means of a predictor-corrector treatment of the source and convective terms. The spatial differences are based on a generalization of the volume-centred discretization method of Mönchmeyer & Müller (1989), due to the incorporation of grid motion. In its standard form, the volume-centred method results in a conservative, second-order preserving scheme in curvilinear coordinates, as was demonstrated through convergence testing. A similar spherical coordinate-based code was previously implemented by Boss & Myhill (1992) who showed that with the use of volume-centred differences, spatial second-order accuracy can be achieved in actual 3D collapse calculations - at least over the range of spatial resolution where 3D runs can be made in practice - without the need of using directional splitting techniques for treatment of the convective terms, as advocated by Finn & Hawley (1989). In collapse calculations with Boss & Myhill's (1992) code, adequate central resolution is maintained by means

of a grid redefinition procedure, and so most of the good properties of the volume-centred method are preserved in a direct manner. Here, spatial resolution is maintained by allowing the radial grid to move with matter, and hence in order to preserve the second-order properties of the volume-centred method, a new FD formulation is used to correctly design the convective terms. It consists of appropriate geometrical and temporal corrections which make the hydrodynamical transport algorithm numerically invariant under grid motion, thereby yielding numerical solutions that are free of a class of systematic errors introduced when standard FD replacements are used on moving grids. This new approach is seen to result in a high degree of accuracy on the pressureless collapse test case. Consistent advection (Norman, Wilson & Barton 1980) is also implemented in the definition of the convective fluxes, and transport of mass is performed using a generalization to spherical coordinates of the van Leer (1977) monotonic interpolation method. This results in good local conservation of angular momentum for axisymmetric flows. An artificial viscosity, based on the tensor formulation of Tscharnuter & Winkler (1979), is added to improve stability against shock formation. A more detailed description of the code and results from a variety of tests is under preparation, and will be presented in a forthcoming paper (Sigalotti 1996).

The standard test model calculation is made using a spherical grid consisting of $1+n_r = 51$ initially uniformly distributed radial points (including the origin $r = 0$), $2 + n_\theta = 87$ fairly equidistant points for $0 \leq \theta \leq \pi$ (including the rotation axis $\theta = 0, \pi$), and $n_\phi = 80$ uniformly spaced points along the azimuthal coordinate for $0 \leq \phi \leq 2\pi$. This resolution corresponds to a total number of $1 + n_r(2 + n_\theta n_\phi) = 340101$ effective cells filling the entire computational volume. Reflection symmetry through the equatorial plane ($\theta = \pi/2$) is assumed so that only the top hemisphere is represented by the calculation ($1+n_\theta = 44$ cells for $0 \leq \theta \leq \pi/2$). At the surface ($r = R$) of the spherical grid, we enforce a constant-volume boundary condition by setting a zero radial velocity. Thus adequate inner resolution is achieved by allowing all interior radial points to contract during the main collapse phase while keeping the external radius fixed in space and time. For this model, the code was able to handle the gradients which formed in the late evolution without the need of the artificial viscosity and so it was never used throughout the calculation. With this choice of the numerical techniques, the standard test model evolved for $\sim$ 32000 time steps corresponding to about 180 hr of CPU time on a CRAY J916/6 supercomputer.

In order to test the code at much lower initial grid resolution, the standard collapse model was rerun with $1 + n_r = 41$ radial points, $2 + n_\theta = 45$ points for $0 \leq \theta \leq \pi$ (i.e., $1 + n_\theta = 23$ points for $0 \leq \theta \leq \pi/2$ because of the assumption of equatorial symmetry), and $n_\phi = 32$ points for $0 \leq \phi \leq 2\pi$. This resolution amounts to a total number of 55121 effective cells which is a factor of $\sim$ 6 lower than the total number of cells allowed in the high-resolution calculation. Hereafter we shall refer to the low- and high-resolution runs as model FDl and model FDh, respectively.

2.3. Code TREESPH

The version of code TREESPH used for the calculations of this paper is a descendant of the scheme originally formulated by Hernquist & Katz (1989). The code combines the method of SPH developed by Lucy (1977) and Gingold & Monaghan (1977) with the hierarchical tree algorithm of Hernquist (1987) for the calculation of the gravitational potential. Basically, the SPH method is a grid-free Lagrangian scheme in which the mass-density as well as all other physical properties of the fluid are determined from the properties of a quasi-random sample of a finite number of fluid elements (particles) through kernel estimation. In TREESPH, the mean value of a field quantity, say the mass-density $\rho(\mathbf{r})$, within a volume element of extent h, is fully determined by means of a symmetrized smoothing procedure using the spherically symmetric spline kernel $W(r, h)$ proposed by Monaghan & Lattanzio (1985). The parameter h, known as the smoothing length, gives the local spatial resolution. A temporally and spatially varying h is used so that regions of the flow with relatively low and high density of particles can be solved with comparable accuracy. Since the mean density is evaluated through kernel estimates, the continuity equation is satisfied automatically to second order in h and so it need not be solved. The positions $\mathbf{r}$ and velocities $\mathbf{v}$ of particles are determined by solving the Euler's equation

$$\frac{d\mathbf{r}}{dt} = \mathbf{v} \quad , \tag{2}$$

$$\frac{d\mathbf{v}}{dt} = -\frac{1}{\rho}\nabla p - \nabla\Phi + \mathbf{A}_{vis} \quad , \tag{3}$$

where p, Φ, and $\mathbf{A}_{vis}$ denote, respectively, the gas pressure, the gravitational potential, and the artificial viscous acceleration associated with the particles. Equations (2) and (3) are complemented by a further equation for the specific internal energy. However, this equation is not used in the calculation of the standard test case because of the assumption of a barotropic equation of state $p \propto \rho$. The form of the artificial viscosity and the symmetrized smoothed representation of the pressure gradient are as given in Hernquist & Katz (1989). The gravitational acceleration term is calculated using the TREECODE of Hernquist (1987), which is an optimized Fortran implementation of the tree method of Barnes & Hut (1986). The details of this code are described in full in Hernquist (1987) and references therein. The time integration of Eqs. (2) and (3) is made explicitly using a second-order accurate leapfrog scheme. In doing so, each particle is allowed to have its own time step which is limited to maintain stability according to a modified form of the Courant condition. In TREESPH, the individual particle time steps are further constrained to be a fraction of the largest system time step Δt_s, which enters as an input parameter.

In this standard formulation, however, the use of time-varying smoothing lengths can lead to a violation of the fluid conservation laws in certain extreme situations. This was first made evident by Hernquist (1993) who showed that during a head-on collision between two identical polytropes, errors in the conservation of the total energy or entropy may occur at

a level of $\sim$ 10%, depending on whether the internal energy or the entropy equation is integrated. A new SPH formulation, which results in a conservative scheme even with the use of varying smoothing lengths, has been introduced by Nelson & Papaloizou (1993, 1994). Basically, this new formulation differs from that of Hernquist & Katz (1989) in that correction terms that account for the variability of the smoothing lengths, the ∇h terms, are added to the usual smoothed representation of the particle equations of motion and internal energy, with h being now prescribed to be a function of the interparticle distances. The inclusion of the ∇h terms had the effect of reducing the non-conservation errors to $\sim 1\%$ in a head-on collision test, irrespective of whether the internal energy or the entropy equation is integrated. An alternative SPH formulation, which also results in improved conservation properties for adiabatic flows, was independently proposed by Steinmetz & Müller (1993). In the case of barotropic (isothermal) flows, entropy conservation is no longer required as entropy is not conserved in isothermal systems, and only the particle equations of motion need be corrected. However, isothermal collapse test calculations by Nelson & Papaloizou (1993) showed that including the ∇h terms in the equations of motion, although it resulted in improved total energy conservation, had little effect on the qualitative outcome of the results. Therefore, for the purposes of the present study we omit the use of the ∇h terms and rely on the standard SPH formulation of Hernquist & Katz (1989). Code TREESPH has been used for a variety of other tests, and results from them together with the description of a modified implemented version of the SPH part of the code will be presented in an oncoming paper (Klapp 1996).

We present two separate model calculations of the standard test case with code TREESPH which differ only in the number of initial particles (N=7123 and N=13997). Similar sets of particles were used by ML in their SPH calculations for the same system. The initial protostellar cloud is set up by first defining a Cartesian box of sides $X = Y = Z = 2R$, where R is the initial radius of the cloud. The box is then filled up with regular cubic cells, each of volume Δ^3, and the origin ($x = y = z = 0$) of the Cartesian grid is made to coincide with the vertex common to the eight central cells (geometrical centre of the square box). An approximate sphere of radius R is then obtained by placing the particles at the cell vertices at distances $d \leq R$ from the origin. Thus the region surrounding the sphere is a vacuum. The azimuthal density perturbation (1) is added by assigning to each particle q a mass given by

$$M_q = \frac{M}{N}\left[1 + a\cos\left(m\phi_q\right)\right] \quad , \tag{4}$$

where $M = 1M_\odot$ is the total mass of the sphere, N is the total number of particles inside the spherical volume, and the parameters a and m are as given in §2.1. The initial cloud is assumed to be at rest except for rotation and so the particle at (x_q, y_q, z_q) is assigned an initial velocity given by

$$\begin{aligned} v_x(q) &= -\omega_0 \cdot y_q \quad , \\ v_y(q) &= +\omega_0 \cdot x_q \quad , \\ v_z(q) &= 0 \quad , \end{aligned} \tag{5}$$

where ω_0 is the initial uniform angular velocity defined in §2.1. The smoothing length of particle q, say h_q, is adjusted such that it is allowed to interact with a constant number $n = 30$ of nearby particles lying within a radius $2h_q$. The largest system time step is chosen to be $\Delta t_s \approx 8 \times 10^7$ s for both calculations. With $N = 7123$ particles the code requires about 7 s/cycle and with $N = 13997$ it requires about 14 s/cycle on a CRAY YMP-4 supercomputer.

3. Results

3.1. Comparison between the FD and the TREESPH evolution

The sequence of equatorial density contours of Fig. 1 shows the time evolution undergone by model FDh. For all of the model calculations the time is measured in units of the initial free-fall time for collapse t_{ff} ($t_{ff} = \sqrt{3\pi/32G\rho_0}$, where ρ_0 is the initial reference density). By comparison, Fig. 2 displays a similar sequence of contour plots for the same evolution, as calculated with code TREESPH using $N = 13997$ particles. An essentially identical sequence was obtained using $N = 7123$ particles. Since no assumptions about symmetry were made in the TREESPH calculations, the plots of Fig. 2 refer to the (x, y)-plane containing the particle of maximum density. The contours are then obtained by projecting onto that plane the positions of all particles within the range $(-z_0, +z_0)$, where z_0 is defined to be a small fraction f of the initial cloud radius. We choose $f = 0.005$ for the $N = 13997$ calculation and $f = 0.02$ for the lower resolution run ($N = 7123$).

In spite of differences in the numerical methods and set up of the initial conditions, both calculations agree that up to the time they could be compared, the result of the evolution is the formation of a protostellar binary system. The intermediate forms of the collapse are also seen to compare qualitatively well. Due to the rapid rotation ($\beta = 0.20$) assumed for the standard isothermal test case, the cloud collapses to form a rotationally flattened disk about the equatorial plane. Meanwhile, direct fragmentation into a binary system occurs as a result of the gravitational growth of the initial $m = 2$ density perturbation. Fig. 3 shows the evolution of the maximum amplitude of the first four even modes ($m = 2, 4, 6, 8$) in a Fourier expansion of the equatorial density for model FDh. The $m = 2$ mode amplifies slowly during the first half of the free-fall time and thereafter it grows more rapidly reaching amplitudes of ~ 1.7 by $1.20t_{ff}$. Substantial growth of the higher order modes is seen to occur only after about $1.0t_{ff}$ with maximum amplitudes $1.0 < a < 1.5$ by the end of the calculation. As expected, the odd modes always kept down at a level of noise with maximum amplitudes $\lesssim 10^{-4}$.

Contrary to previous first-order calculations, no intermediate bar configuration forms in the present models. This feature was first noted by MB who compared results for the standard isothermal test case from two different second-order FD codes: one based on Cartesian coordinates and the other on spherical coordinates. Their results with the spherical coordinate code, however, indicate that in spite of the second-order accurate

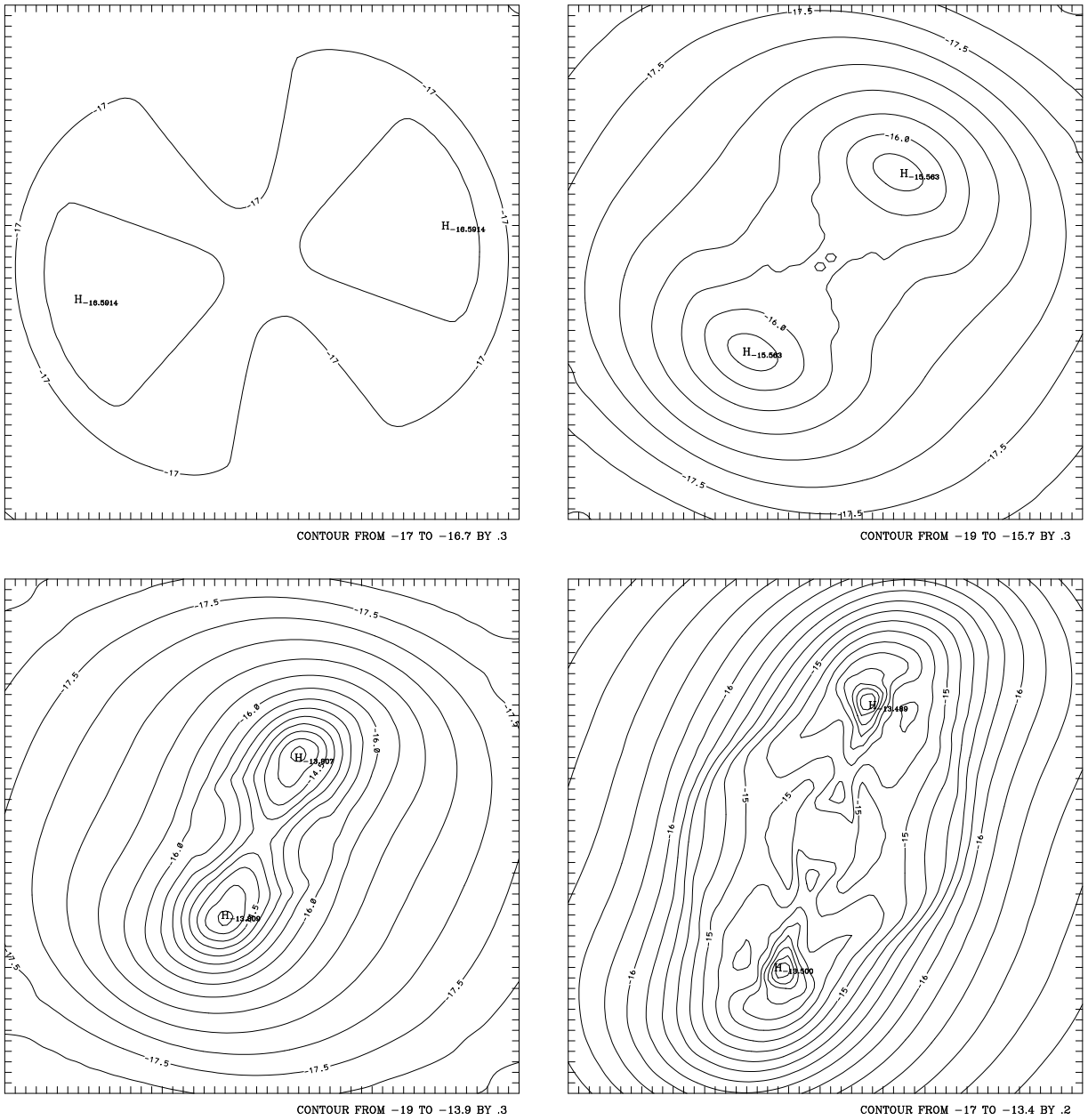

Fig. 1a–d. Equatorial density contours for the standard isothermal collapse test, as obtained for model FDh. The contour lines correspond to the logarithm of the density. The high-density value is labeled. Counterclockwise rotation is assumed. A sequence in time is presented: **a** (upper left) $0.284t_{ff}$, **b** (upper right) $0.913t_{ff}$, **c** (lower left) $1.112t_{ff}$, and **d** (lower right) $1.240t_{ff}$. The entire cloud is shown in **a**-**c**. A region of radius 2.0×10^{16} cm is shown in **d**.

methods, an intermediate bar may eventually form if the allowed equatorial resolution is not adequate to solve the rotationally flattened disk forming from collapse. In particular, using a θ-grid with $n_\theta = 23$ fairly equidistant points for $0 \leq \theta \leq \pi/2$, the evolution was seen to pass through an intermediate bar configuration as in previous first-order calculations while, for the same n_θ, the intermediate bar disappeared when the calculation was repeated using a stretched (non-uniform) θ-grid about the equatorial plane, thereby allowing finer resolution there at the expense of much coarser resolution near the rotational axis. The non-uniform θ-grid (with $\Delta\theta_j = 1.2\Delta\theta_{j-1}$) used in MB gives an angular spacing, $\Delta\theta_2 = \theta_2 - \theta_1 \equiv \theta_2 - \pi/2$, near the equatorial plane which is a factor of 6 smaller than the corresponding one allowed in the calculation of model FDh (with $n_\theta = 44$ fairly equidistant points for $0 \leq \theta \leq \pi/2$). In spite of this difference in equatorial resolution, the contours of Fig. 1 closely resemble those given in MB at comparable maximum densities. This result clearly indicates that the disappearance of the intermediate central bar is a consequence of the smaller diffusive truncation errors associated with code FD, and that

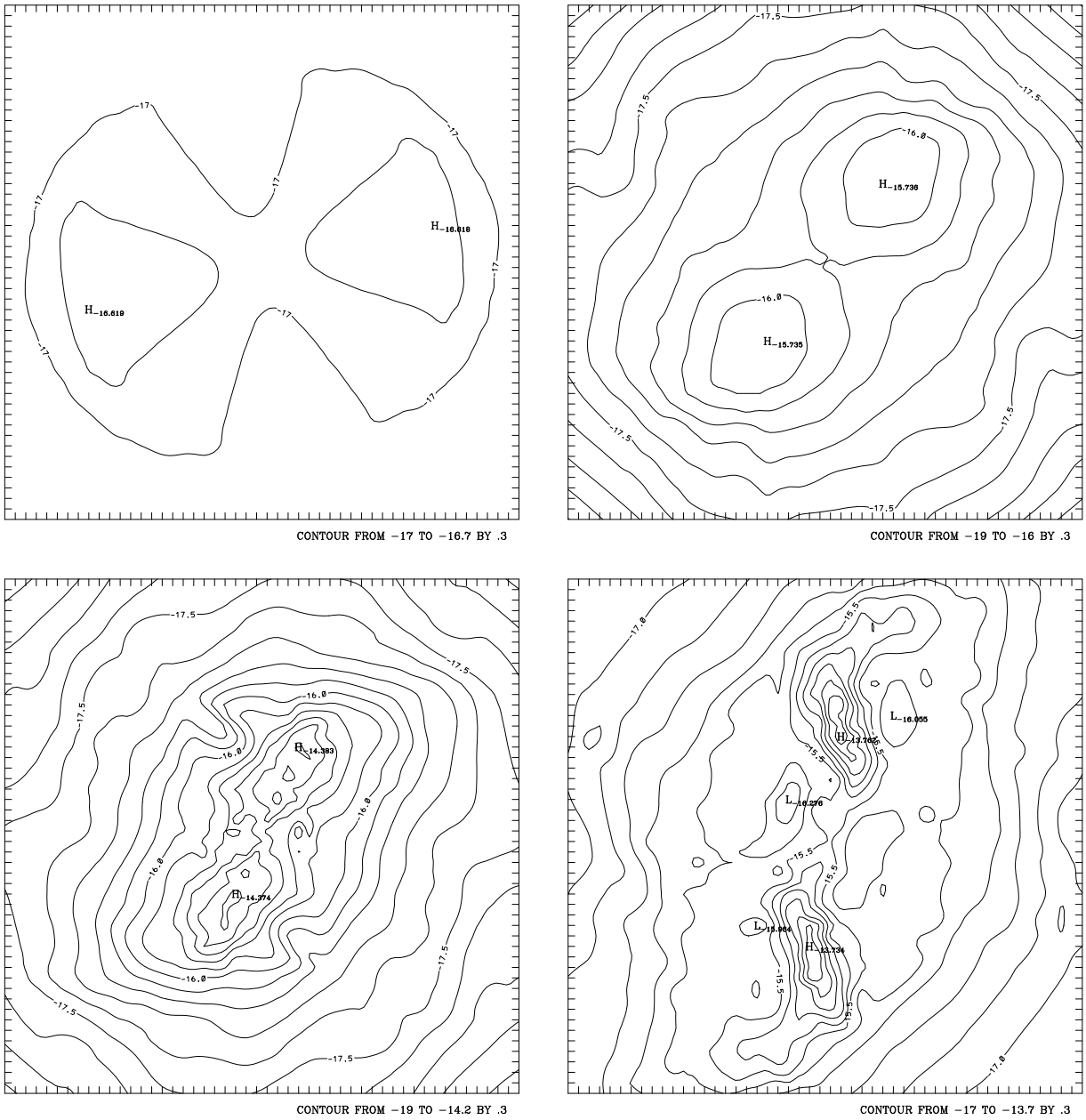

Fig. 2a–d. Equatorial density contours for the standard isothermal collapse test, as calculated with code TREESPH using 13997 particles. The contour lines correspond to the logarithm of the density. The high-density value is labeled. Counterclockwise rotation is assumed. A sequence in time is presented: **a** (upper left) $0.217t_{ff}$, **b** (upper right) $0.932t_{ff}$, **c** (lower left) $1.142t_{ff}$, and **d** (lower right) $1.329t_{ff}$. The entire cloud is shown in **a**-**c**. A region of radius 2.0×10^{16} cm is shown in **d**. An essentially identical sequence was obtained using 7123 particles.

enhanced equatorial resolution plays a minor role in determining that feature. This last statement is further confirmed by the results obtained for model FDl, with n_θ = 23 fairly equidistant points for $0 \leq \theta \leq \pi/2$ as in the spherical coordinate model in MB that produced an intermediate bar. The evolution of this model is illustrated in the sequence of contour plots of Fig. 4. Although this calculation was made with lower initial radial and azimuthal resolution (i.e., $1 + n_r$ = 41 and n_ϕ = 32) compared to model FDh and the calculations in MB, we see that the intermediate forms of collapse are very similar to those shown in Fig. 1 and that again no bar configuration is seen to form. The growth of the maximum equatorial amplitude of the first four even modes closely follows that given in Fig. 3, with the m = 2 mode reaching amplitudes of $\sim$ 1.79 by the end of the calculation ($\sim 1.32t_{ff}$). Furthermore, comparison of the results from the TREESPH calculations shows that varying the number of particles has also little effect on the intermediate forms of the evolution. In both of these model calculations, the protostellar binary formed by direct fragmentation without the occurrence of an intermediate central bar (see Fig. 2).

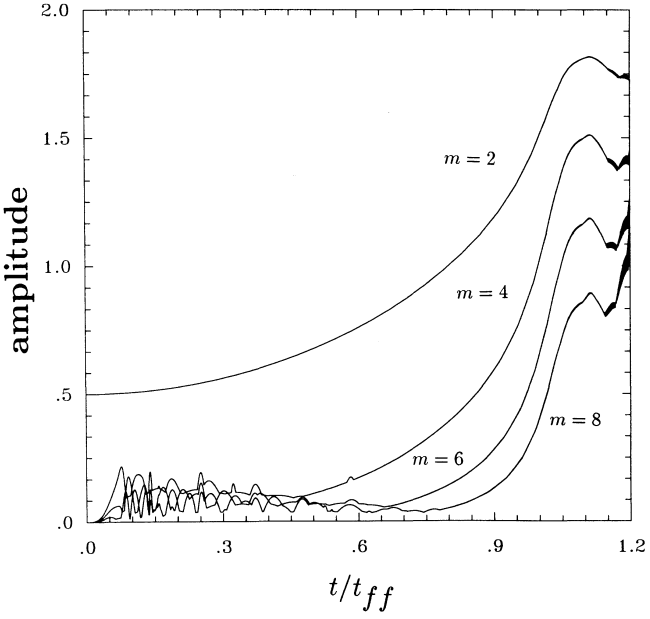

Fig. 3. Growth of the maximum amplitude of modes $m = 2, 4, 6, 8$ in the equatorial plane for the calculation of model FDh. Odd modes kept down at a level of noise with maximum amplitudes $\lesssim 10^{-4}$.

The variation of the maximum density with time is shown in Fig. 5. The results indicate that the maximum density is much less sensitive to resolution than was previously found by ML. We see that the TREESPH sequence with 13997 particles closely follows that with 7123 particles, the former showing slightly higher maximum densities only after the first free-fall time. The effects of resolution are made more evident by intercomparing the FD sequences, where at comparable phase the differences in maximum density are larger. Although the maximum density in model FDh is always above that of the TREESPH sequences, the trends of the time variation are very similar. The major differences between the FD and the TREESPH sequences are seen to occur after about $1.10t_{ff}$ when the evolution of the fragments is dominated by their internal forces. These differences, however, cannot be explained solely in terms of differences in the final resolution achieved by the two methods. Indeed we find that the TREESPH calculations produce forming-fragment regions with a relatively higher rotational energy ($\beta_f \gtrsim 0.31$ by $\sim 1.10t_{ff}$) compared with the FD models. Thus the central regions of the TREESPH fragments may become rotationally unstable and bounce, giving rise to a temporary decrease of the maximum density. The excess of rotation at the centre of the FD fragments was less severe but still enough to produce a slow collapse. This explains the much milder increase of the maximum density for the FD sequences after $\sim 1.10t_{ff}$. During this phase, the gravitational energy at the centre of the fragments has sufficiently increased to induce a more rapid collapse, as evidenced by the further sudden rise of the maximum density. A similar behaviour is also observed to occur in the evolution of the TREESPH fragments but on a relatively longer time-scale. This is because the fragments must dispose of their excess of rotational energy before trying to collapse upon themselves. Transfer of angular momentum to the spiral arms is the likely mechanism through which the TREESPH fragments may eventually reduce the importance of the rotational energy and collapse to higher densities.

Another interesting question regarding the standard isothermal collapse test case is whether or not the evolution will result in a run-away collapse of the fragments. The results with code TREESPH show that the fragments may evolve farther in time without undergoing rapid collapse upon themselves, in good agreement with ML calculations. This aspect was in contrast with the results from early first-order FD calculations, where as suggested by ML, run-away collapse occurred because the description of the fragments could have been degraded by the excessive numerical diffusion of angular momentum from them. However, the results with code FD indicate that in spite of the decreased numerical diffusion associated with the second-order methods, the description of the fragments can also critically depend on spatial resolution. This aspect is made evident in Fig. 5, where in the case of model FDh the maximum density suddenly stops increasing at $\sim 1.20t_{ff}$ and thereafter starts oscillating as in the TREESPH calculations, while at comparable values, the maximum density in the sequence of model FDl continues increasing, indicating a run-away collapse of the fragments as in all previous first-order calculations. Unfortunately, the calculation of model FDh was halted shortly after (at $\sim 1.26t_{ff}$) because the time steps became extremely small. On the contrary, the calculation of model FDl was continued up to $\sim 1.32t_{ff}$ when $\rho_{max} \approx 4680\rho_0$. By this time, however, the accuracy of the evolution has already been degraded due to the lack of resolution as the fragments rapidly concentrated in a few grid cells. The TREESPH calculations were terminated at $1.80t_{ff}$ to allow comparison with ML results for the long term evolution.

The density contours of Fig. 1d (at $1.24t_{ff}$) and 2d (at $1.33t_{ff}$) show the protostellar binary resulting from the high-resolution calculations with code FD and code TREESPH, respectively. The maximum density in Fig. 1d is $\rho_{max} \approx 3550\rho_0$ and that in Fig. 2d is $\rho_{max} \approx 2250\rho_0$. The general shape of the density contours in Fig. 1d is very similar to that given in MB. Because of the higher azimuthal resolution used here ($n_\phi = 80$ against $n_\phi = 64$ in MB and $n_\phi = 32$ for model FDl), the binary fragments evolved on a slightly shorter time-scale. The fragments obtained with code TREESPH appear to have an elongated shape and resemble the ML fragments more closely than those found with the FD codes. The presence of well-defined spiral arms just outside the main fragments is also evident in Fig. 2d. These features are also present in Fig. 1d but in a less prominent fashion. We further note that despite these differences, the time-scale and the maximum densities for the TREESPH evolution closely agree with those given in MB using their Cartesian FD code.

The final shape of the fragments may be influenced by the accretion of matter from the outer cloud regions. The accretion process is clarified in Figs. 6 and 7, which show the velocity field in the equatorial plane at the times of Figs. 1d and 2d, respectively. We see that the accretion is highly anisotropic with

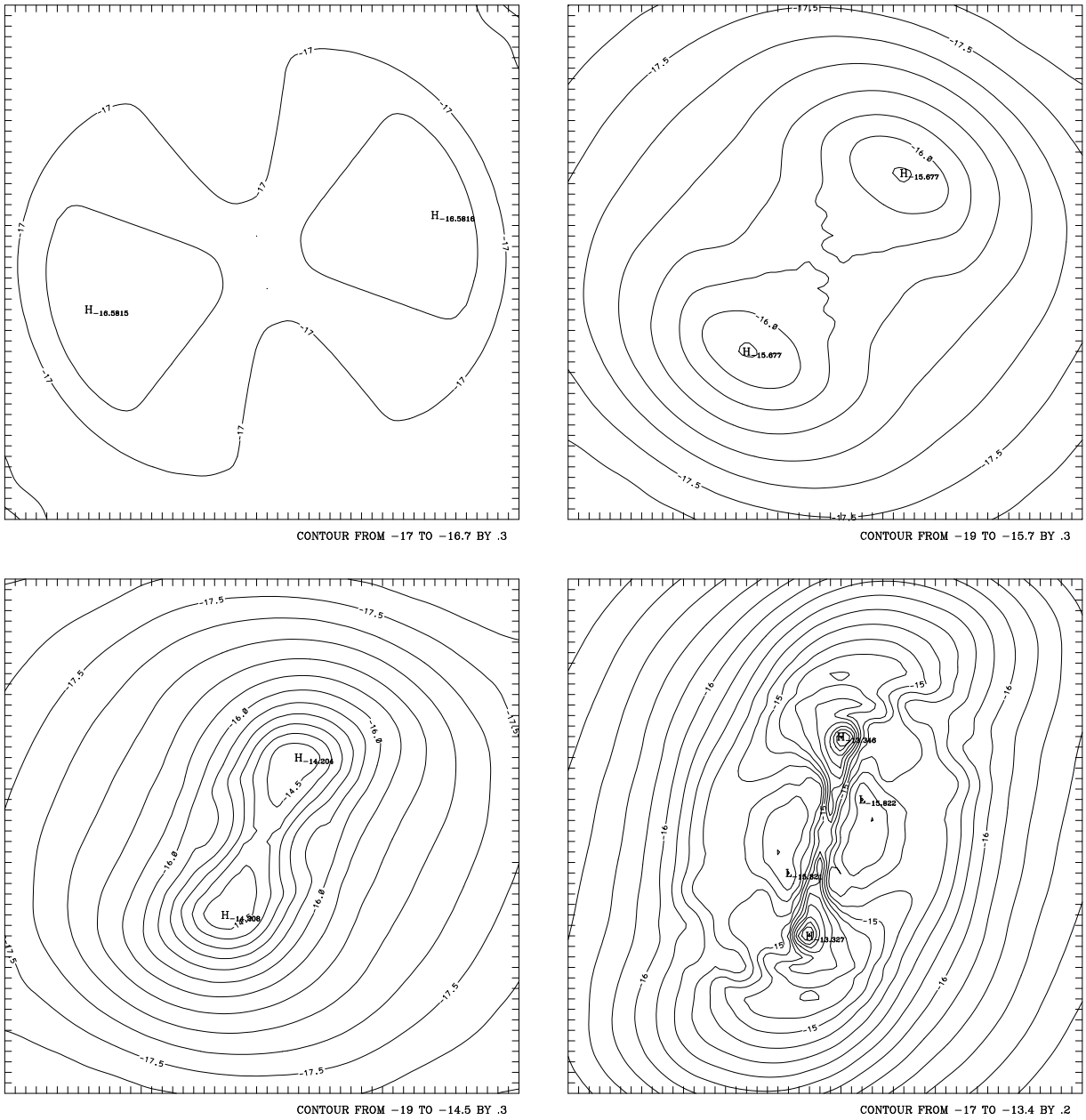

Fig. 4a–d. Equatorial density contours for the standard isothermal collapse test, as obtained for model FDl. The contour lines correspond to the logarithm of the density. The high-density value is labeled. Counterclockwise rotation is assumed. A sequence in time is presented: **a** (upper left) $0.314t_{ff}$, **b** (upper right) $0.899t_{ff}$, **c** (lower left) $1.125t_{ff}$, and **d** (lower right) $1.305t_{ff}$. The entire cloud is shown in **a**-**c**. A region of radius 2.0×10^{16} cm is shown in **d**.

strong pressure gradients forming preferentially in the azimuthal direction. These gradients involve a sharp transition from supersonic to subsonic velocities as shown more clearly in Fig. 6. The matter which approaches the fragments azimuthally, i.e., in the sense of the general cloud rotation (downstream matter), loses angular momentum due to the gravitational attraction exerted by the fragment and then swings inwards. Most peripheral mass with high angular momentum is seen to swing further outwards and then to approach the fragment on curved trajectories (upstream matter). While these features are essentially the same in Figs. 6 and 7, there is still a basic difference between them - accretion of mass onto the TREESPH fragments occurs preferentially through the spiral arms. This would explain their more elongated shape, which is also evident in Fig. 7 as shown by the regions where the velocity arrows are heavily superimposed. Furthermore, the fragments produced here look quite flattened about the equatorial plane and surrounded by a planar shock through which they accrete low angular momentum mass in the z-direction.

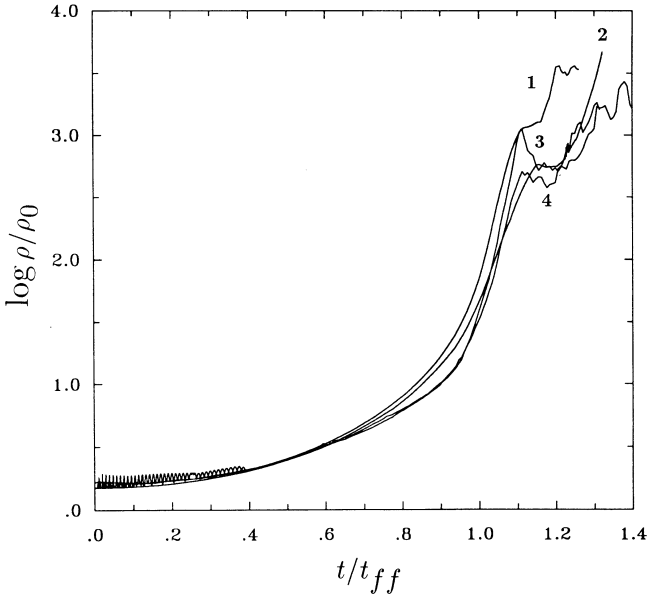

Fig. 5. The variation of maximum density with time, as calculated with code FD (curve 1: model FDh; curve 2: model FDl) and with code TREESPH using 13997 (curve 3) and 7123 (curve 4) particles.

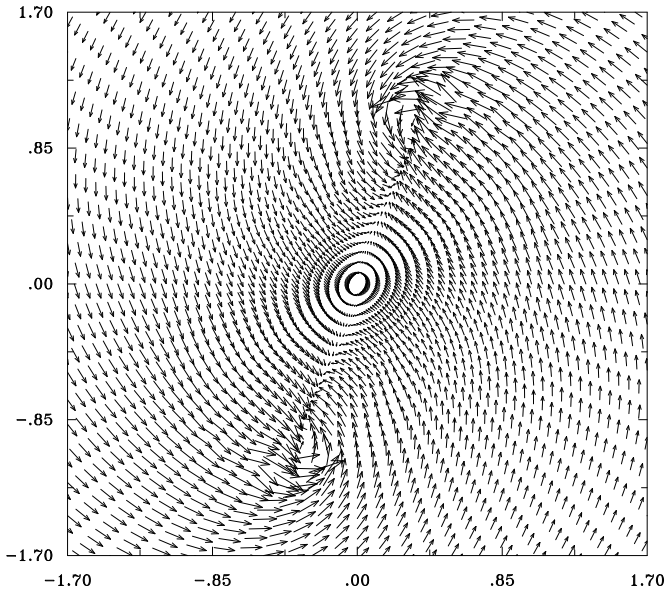

Fig. 6. Velocity field in the equatorial plane at $1.240t_{ff}$, for model FDh. The rotation axis is in the centre of the plot. The numbers on the box sides are given $\times 10^{16}$ cm. The maximum velocity is 1.55 km s^{-1}.

3.2. Integral properties of the fragments

In numerical calculations of protostellar collapse and fragmentation we are always concerned with the properties of the resulting fragments. Here the fragment region is defined as the cell (or particle) of maximum density, plus all surrounding cells (or particles) with densities higher than a factor $1/f_D$ of the maximum value. For simplicity, in the sequel we shall refer to these cells (FD case) and particles (TREESPH case) as the elements making up the fragment. The total mass of the fragment M_f is then determined by summing up the masses of the individual elements. The internal velocity field of the fragment, say $(v'_r, v'_\theta, v'_\phi)$, is here defined with respect to a spherical coordinate system (r', θ', ϕ') whose origin ($r' = 0$) coincides with the instantaneous location of the element of maximum density (centre of the fragment). In this frame, the fragment's rotation axis ($\theta' = 0$) is assumed to be perpendicular to the equatorial plane of the cloud. These velocities should not be confused with those describing the internal motion of the cloud (v_r, v_θ, v_ϕ) with respect to its centre of mass $\mathbf{R}_{CM}$ (see Figs. 6 and 7). In the FD calculations, $\mathbf{R}_{CM}$ was always seen to coincide with the origin ($r = 0$) of the grid coordinate system (r, θ, ϕ). In the TREESPH calculations, equatorial symmetry is well maintained and $\mathbf{R}_{CM}$ is found to lie approximately in the (x, y)-plane containing the particle of maximum density, with $d\mathbf{R}_{CM}/dt \approx 0$ during the evolution. Therefore we can always define a spherical coordinate system (r, θ, ϕ) with origin at $\mathbf{R}_{CM}$ and with respect to which the actual particle velocities are assumed to be defined. Thus the location (r', θ', ϕ') of an element relative to the fragment's centre can be determined from its location (r, θ, ϕ) with respect to the cloud's centre by means of the transformations

$$r' = \left(r^2 + r_f^2 - 2rr_f \cos\psi\right)^{1/2} \quad ,$$

$$\sin\theta' = \frac{1}{r'}\left(r^2 \sin^2\theta + r_f^2 - 2rr_f \cos\psi\right)^{1/2} \quad , \tag{6}$$

$$\tan\phi' = \frac{r\sin\theta\sin\phi - r_f \sin\phi_f}{r\sin\theta\cos\phi - r_f\cos\phi_f} \quad ,$$

where $\cos\psi = \sin\theta\cos(\phi_f - \phi)$, and $(r_f, \theta_f = \pi/2, \phi_f)$ are the coordinates of the element of maximum density. Differentiating with time the above relations gives the velocity of the fragment element $(v'_r = \dot{r}', v'_\theta = r'\dot{\theta}', v'_\phi = r'\sin\theta'\dot{\phi}')$ in terms of its components (v_r, v_θ, v_ϕ) and the velocity of the element of maximum density $(v_{r_f} = \dot{r}_f, v_{\theta_f} = 0, v_{\phi_f} = r_f \sin\theta_f \dot{\phi}_f)$ as measured in the main cloud frame. Let now consider the equatorial plane of the cloud, as shown in Fig. 6, and assume that the binary fragment produced is such that its centre (point of maximum density) has $v_{r_f} = v_{\phi_f} = 0$. In this case, we recover the identity $v'^2_r + v'^2_\phi = v_r^2 + v_\phi^2$, and if we further assume that the elements of the fragment are only undergoing rotational motion about its axis of spin ($\theta' = 0$), then $v'_r = 0$ and $v'^2_\phi \equiv v_r^2 + v_\phi^2$. We see from Fig. 6 that this is not the case and that deriving $(v'_r, v'_\theta, v'_\phi)$ as described above is necessary to improve on the accuracy of the rotational properties. The gravitational, thermal, rotational, and kinetic non-rotational energies as well as the spin angular momentum of the fragment J_f are then evaluated by summing the volume-element integrated values of $(1/2)\rho\Phi$, $(3/2)p$, $(1/2)\rho v'^2_\phi$, $(1/2)\rho(v'^2_r + v'^2_\theta)$, and $\rho r' \sin\theta' v'_\phi$, respectively, over all elements composing the fragments. This determines the values of α_f, β_f, and δ_f which denote, respectively, the ratios of the thermal, rotational, and kinetic non-rotational to the gravitational energy for the clumps. Finally, the spin specific angular momentum of the fragment $(J/M)_f$ is found by dividing its spin angular momentum J_f by its total mass M_f.

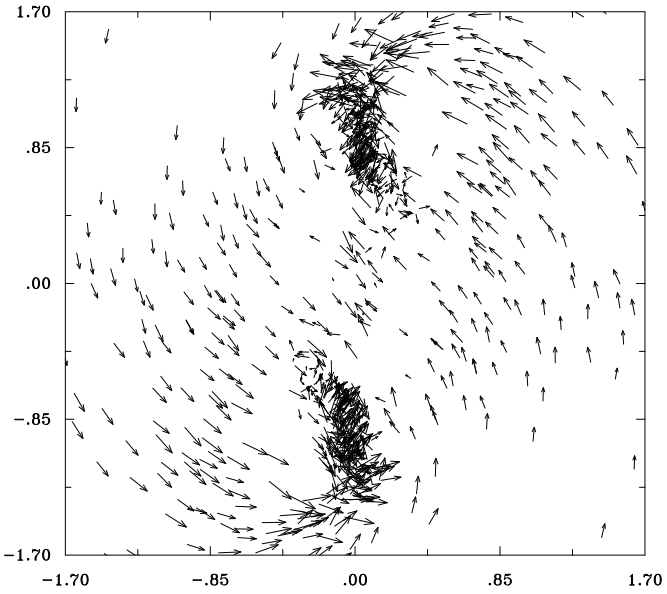

Fig. 7. Velocity field in the equatorial plane at $1.329t_{ff}$, as calculated with code TREESPH using 13997 particles. The numbers on the box sides are given $\times 10^{16}$ cm. The maximum velocity is 1.26 km s^{-1}. Only particles within a fraction $f = 0.005$ of the initial cloud radius above and below the equator are shown.

Table 1. Fragment properties for $f_D = 10$: comparison with previous calculations

Model	$M_f/M_\odot$	α_f	β_f	δ_f	$(J/M)_c/(J/M)_f$	$\frac{1}{2}D_{bin}/R$	t/t_{ff}
B32	0.14	0.04	0.20	- -	14	0.18	1.42
T32	0.15	0.03	0.15	- -	23	0.20	1.42
FS32	0.14	0.09	0.22	- -	13	0.18	1.43
M64	0.15	0.08	0.29	- -	10	0.28	1.32
B64	0.10	0.13	0.38	- -	12	0.32	1.32
BBPi	0.17	0.02	0.24	- -	12	0.29	1.32
BBPp	0.17	0.10	0.28	- -	12	0.29	1.32
S32	0.11	0.06	0.10	0.17	11	0.25	1.31
S80	0.09	0.06	0.23	0.09	10	0.34	1.24
K7123	0.05	0.09	0.29	0.07	11	0.32	1.33
K13997	0.05	0.08	0.26	0.10	14	0.29	1.33

We have calculated the properties of the binary fragments for two different choices of the factor $1/f_D$. In Table 1, we use $f_D = 10$ and compare our results (S32 and S80: code FD; K7123 and K13997: code TREESPH) with those from previous first-order donor-cell calculations by Bodenheimer & Boss (1981) and de Felice & Sigalotti 1992 (B32: Boss' code with $n_\phi = 32$; T32: Tohline's code with $n_\phi = 32$; FS32: Sigalotti's code with $n_\phi = 32$), second-order FD calculations by MB (M64: Myhill's Cartesian code with 64 points; B64: Boss' spherical code with $n_\phi = 64$), and most recent SPH calculations by Bate et al. (1995) using a version of Willy Benz's code with 8024 particles (BBPi: calculation made using an isothermal equation of state; BBPp: calculation made using a polytropic equation of state with $\gamma = 7/5$ for $\rho > 10^{-14}$ g cm^{-3}). In Table 2, we re-calculate the integral properties by setting f_D according to the actual shape of the fragments as given in Fig. 8. The last two columns in Table 1 and rows in Table 2 list the binary separation in terms of the initial cloud radius and the time at which the fragment properties were evaluated. The specific angular momentum of the initial cloud is compared with that of the resulting fragments to determine the reduction factor of the angular momentum. Since the initial conditions produced symmetric binaries, Tables 1 and 2 show the properties of only one fragment.

Table 2. Integral properties of the actual fragments

Model	S32	S80	K7123	K13997
f_D	10.6	16.4	19.7	20.7
$M_f/M_\odot$	0.12	0.12	0.09	0.08
α_f	0.06	0.06	0.09	0.08
β_f	0.12	0.24	0.28	0.27
δ_f	0.18	0.10	0.07	0.12
$(J/M)_c/(J/M)_f$	11	8	11	13
$\frac{1}{2}D_{bin}/R$	0.25	0.34	0.32	0.29
t/t_{ff}	1.31	1.24	1.33	1.33

3.3. Discussion of the results

We note from Table 1 that the second-order calculations resulted in larger binary separations compared with the first-order ones. This is expected because in all of the second-order calculations the cloud is seen to fragment directly into a binary system. On the contrary, the first-order calculations were largely affected by numerical diffusion which acted primarily to inhibit direct fragmentation. In this case, the initial $m = 2$ density perturbation was seen to decay into a central bar configuration. Subsequent collapse and fragmentation of the bar then resulted in a binary system of separation smaller than that found by direct fragmentation. Numerical diffusion of angular momentum from the growing fragments could also explain the lower final values of β_f along with the increased efficiency of angular momentum redistribution compared with the second-order calculations.

Although Table 1 provides a direct comparison of the fragment properties with previous calculations of the standard isothermal collapse test case, we find that our results can be compared more closely using Table 2, where the properties account for the actual shape of the fragments (see Fig. 8). Considering the differences between the numerical methods, we see that there is a general good agreement between the FD and the TREESPH results. The fragments which form have low values of α ($\alpha_f \lesssim 0.09$) and relatively high values of β ($\beta_f \gtrsim 0.24$). Significant non-rotational motion is also present in their internal structure as suggested by the moderate values of δ ($\delta_f \sim 0.10$). Note that the fragments produced in model FDl have much lower values of β ($\beta_f \sim 0.12$) and higher δ ($\delta_f \sim 0.18$), which is consistent with these clumps being undergoing run-away collapse. All four of our model calculations agree that about 20 percent of the total cloud mass is in the form of fragments, and that their

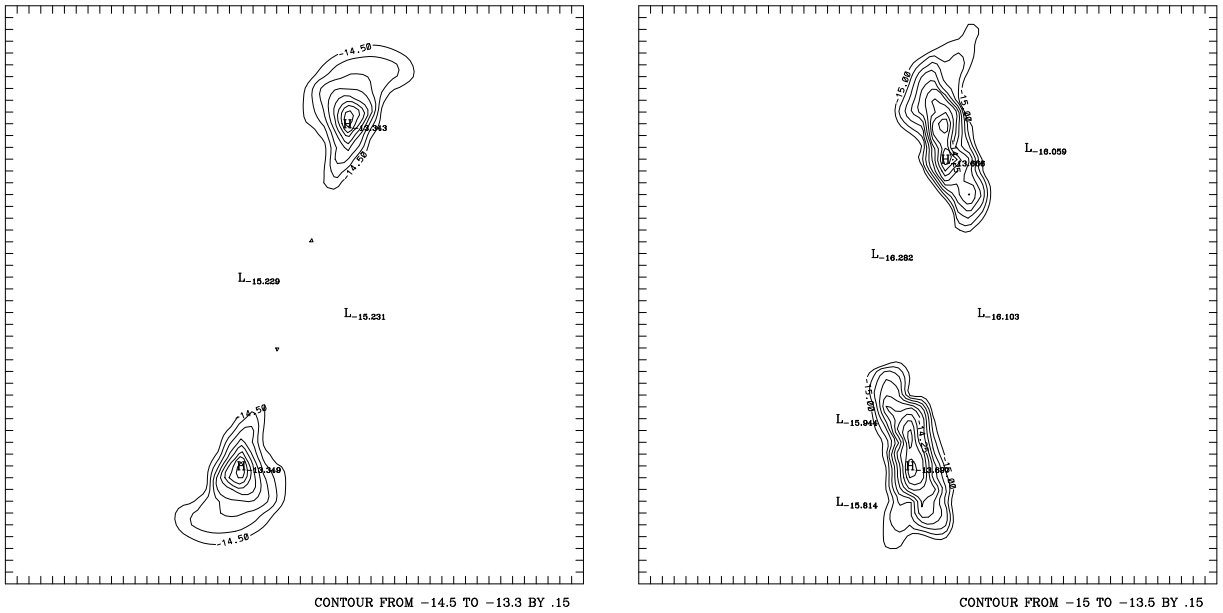

Fig. 8a and b. Equatorial density contours showing the binary fragment region: **a** (left) as in Fig. 1d at $1.240t_{ff}$ (code FD), **b** (right) as in Fig. 2d at $1.329t_{ff}$ (code TREESPH). A region of radius 1.7×10^{16} cm is shown in **a** and **b**. The high- and low-density values are labeled. The m = 2 fragmentary appearance of the fragments in **b** is only a transient feature.

spin angular momentum is not reduced by factors larger than ~ 13 with respect to the initial cloud value.

The fragments are seen to form at such low values of α that they could experience rapid collapse and eventually subfragment in the further evolution. A rapid collapse of the fragments would be accompanied by an equally rapid rise of the maximum density. With the exception of model FDl, our results indicate that the fragments undergo such a rapid collapse until a certain value of the maximum density is reached. Thereafter the collapse slows down and the maximum density may start oscillating. Since we were unable to follow the calculation of model FDh beyond $\sim 1.26t_{ff}$, this trend is barely shown in Fig. 5. Previous SPH calculations by Gingold & Monaghan (1981) and ML, and more recently by Bate et al. (1995), have shown that the long term evolution could be controlled by the gravitational interaction between the two fragments. In ML a clear tendency for the fragments to get closer together was observed to occur up to $\sim 1.95t_{ff}$ when they apparently started to coalesce. A tendency for the fragments to fall towards each other is also seen to occur in our calculations as shown in Fig. 9. In this figure, we plot the time variation of the binary separation (i.e., one-half of the distance between the points of maximum density divided by the initial cloud radius) up to the time the calculations were compared. Although the binary separation is always nearly larger for the FD models, it is seen to decrease at a rate similar to that found in the TREESPH calculations.

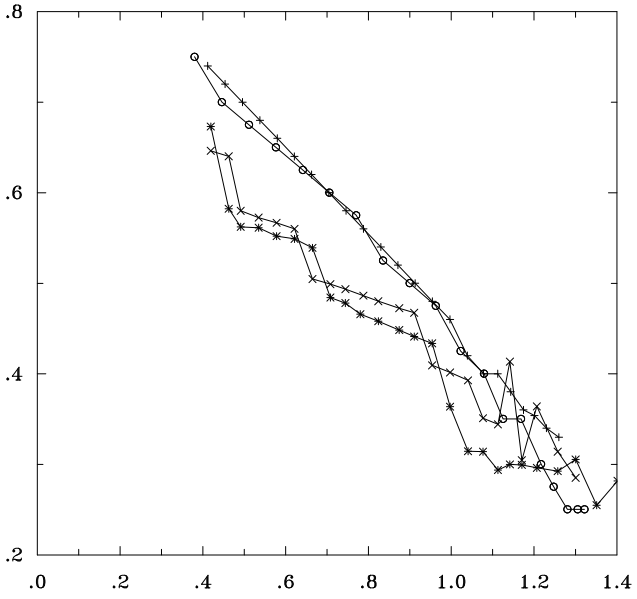

Fig. 9. Variation of the binary separation distance with time, as calculated with code FD (circles: model FDl; plus signs: model FDh) and code TREESPH (asterisks: model with 7123 particles; crosses: model with 13997 particles). The binary separation is measured as one-half of the distance between the points of maximum density divided by the initial cloud radius.

The long term evolution was also studied by Bate et al. (1995) who followed the calculations well beyond the point where ML estimated the fragments to start coalescing. Following the initial fragmentation, the growing fragments were also seen to get progressively closer together. However, by $\sim 1.90t_{ff}$ when the two fragments reach a minimum separation distance, the binary system have had time to acquire enough orbital angular momentum to prevent merging and force the fragments to pass each other at periastron. Thereafter the

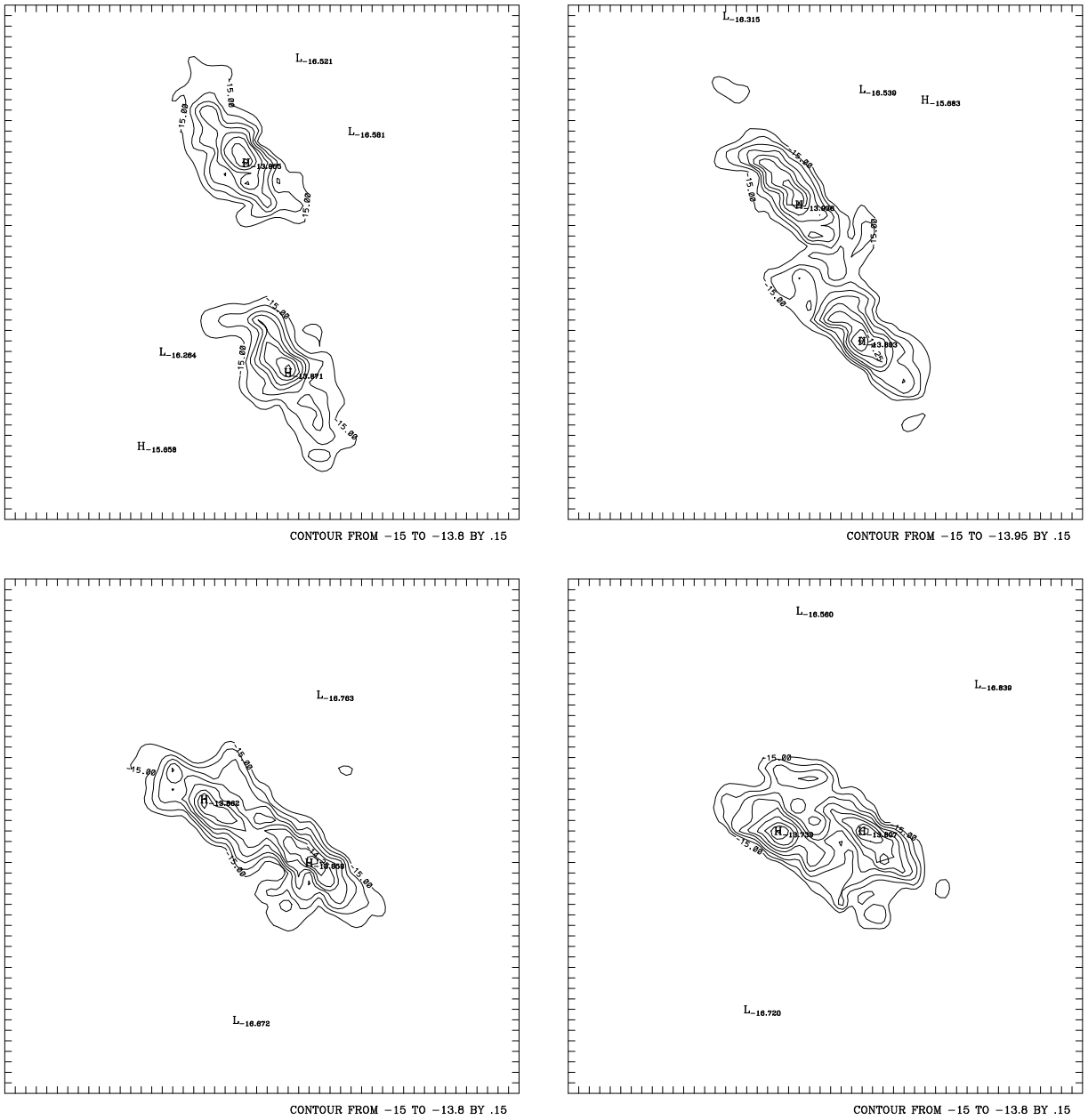

Fig. 10a–d. Equatorial density contours showing the long term evolution of the binary system, as calculated with code TREESPH using 13997 particles. The contour lines correspond to the logarithm of the density. The high- and low-density values are labeled. Counterclockwise rotation is assumed. A sequence in time is presented: **a** (upper left) $1.50t_{ff}$, **b** (upper right) $1.60t_{ff}$, **c** (lower left) $1.73t_{ff}$, and **d** (lower right) $1.80t_{ff}$. A region of radius 1.7×10^{16} cm is shown. The binary separation distance in terms of $\frac{1}{2}D_{bin}/R$ is 0.22, 0.16, 0.12, and 0.09 in **a**, **b**, **c**, and **d**, respectively.

clumps continue to orbit and the disc surrounding one of them fragments into one more object, yielding a triple protostellar system by $\sim 2.20t_{ff}$. The sequence of contour plots in Fig. 10 shows the long term evolution of the binary system up to $1.80t_{ff}$, as calculated with code TREESPH using 13997 initial particles. A similar sequence was also obtained using 7123 particles. As the two clumps approach each other, coalescence at the $\log\rho = -15.0$ contour level is seen to occur by $\sim 1.60t_{ff}$ (Fig. 10b). At this time, the binary separation is a factor of 2 smaller than the value given in Table 2 (Fig. 8b). This trend continues up to $1.80t_{ff}$ as shown in Fig. 10c and d, where coalescence at the four outermost contour levels is evident. Although these results are qualitatively in agreement with the general trends described in ML, we note that by $1.80t_{ff}$, the fragments are still distinct and seem to approach a point of minimum separation without merging, as described in Bate et al. (1995). The question of whether the fragments will definitively merge or survive eventually sub-fragmenting, will require following the evolu-

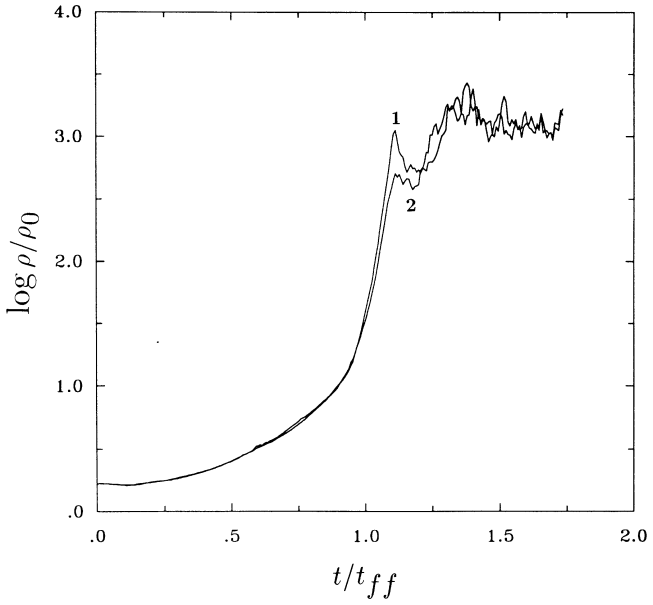

Fig. 11. The variation of maximum density with time as calculated with code TREESPH. Curve 1 refers to the sequence with 13997 particles and curve 2 to that with 7123 particles. The long term evolution is shown up to $1.75t_{ff}$.

tion farther in time than we were able to do here. In any case it seems likely that the protostellar binary is merely a transient feature.

In ML the fragments were estimated to be in approximate equilibrium after $\sim 1.70t_{ff}$ in the long term evolution. We find from Table 2 that at the times when the properties were evaluated, $\alpha_f + \beta_f + \delta_f \approx 0.40$ for the fragments formed in model FDh, and $\alpha_f + \beta_f + \delta_f \approx 0.44$ and 0.47 for those formed in the TREESPH calculations with 7123 and 13997 particles, respectively. While virial equilibrium requires that $\alpha + \beta + \delta = 1/2$, it may well be the case that by these times the outer regions of the fragments are already close to equilibrium and that only a small amount of matter at their centres will continue to collapse. This view is clarified in Fig. 11, where the variation of the maximum density with time is shown up to $\sim 1.75t_{ff}$ for both of our TREESPH calculations. We see that the centre of each fragment undergoes further collapse reaching a maximum density peak by $\sim 1.40t_{ff}$. Thereafter the fragments bounce at their centres and the maximum density begins to oscillate about an equilibrium configuration. During this phase, the evolution of the fragments is clearly influenced by the strong gravitational interaction between them. After $\sim 1.50t_{ff}$, the oscillations of the maximum density produce peaks that are slightly larger in the calculation with 13997 particles. However, later on (by $\sim 1.60t_{ff}$), the oscillations in both sequences start to converge more closely, indicating that the results with respect to run-away collapse of the fragments are reaching the correct continuum limit.

4. Conclusions

We have presented a comparison of the numerical solutions for the standard isothermal collapse test using two independent second-order hydrodynamic codes. One code uses specialized finite-difference techniques on a radially moving, spherical coordinate grid (code FD) and the other is based on the method of smoothed particle hydrodynamics (SPH) coupled with the hierarchical tree algorithm of Hernquist (1987) for the calculation of the gravitational forces (code TREESPH). Two model calculations were run with each code differing only in the initial resolution.

The results indicate that up to the time the calculations could be compared the outcome of the evolution is the formation of a protostellar binary system in agreement with previous calculations of the standard test case. We find that the intermediate forms of the evolution, as calculated with both codes, are very similar and much less sensitive to resolution than was previously found by Monaghan & Lattanzio 1986 (ML). Contrary to previous first-order calculations, here the protostellar binary forms by direct fragmentation, i.e., without the occurrence of an intermediate bar configuration. The disappearance of the intermediate bar was also observed in recent second-order FD calculations by Myhill & Boss (1993), suggesting that this aspect of the solution is a result of the decreased numerical diffusion associated with the new second-order schemes.

Our results show that the basic differences encountered by ML between the finite difference methods and the SPH approach for this problem are actually mitigated. The high-resolution calculation with code FD no longer results in a run-away collapse of the fragments, and as for the TREESPH calculations, the binary companions show a clear tendency to fall towards each other. The fragments are seen to undergo rapid collapse until a certain value of the maximum density is reached. The major differences between the FD and the TREESPH calculations are just observed to occur during this short phase of the evolution. The fragments formed from the FD calculations appear to possess a lower rotational energy and so they collapse on a relatively shorter time-scale with respect to the TREESPH fragments, which must dispose of their excess of rotational energy. These differences in the rotational properties influence the details of the accretion process, which then is seen to determine the observed differences in the final shape of the fragments. The resulting properties of the clumps seem to indicate that their outer regions are very close to equilibrium and that only a small amount of mass at the centre of each fragment may continue to collapse. The results of the long term evolution with code TREESPH confirm this view and show that the central collapse of the fragments may eventually stop. The subsequent evolution is controlled by the strong interaction between them, which halts their collapse to higher densities and forces the binary system to become close enough to eventually coalesce. However, complete coalescence of the fragments is not guaranteed by the present calculations, and as shown by Bate et al. (1995), they could even survive and sub-fragment in the later evolution, leading to the formation of a multiple protostellar

system. These trends suggest that the protostellar binary system could be a transient feature of the overall evolution. Although the calculations with code FD were not continued for such a long time in the evolution, the separation distance between the FD fragments was seen to be decreasing at a rate similar to that found in the TREESPH calculations, and so we may expect the gravitational interaction between the FD fragments to become equally important in the long term evolution.

Acknowledgements. We thank F. de Felice for useful discussions and Lars Hernquist for providing a copy of his TREECODE. We also thank Alan P. Boss for a number of perceptive comments and enlightening suggestions that have certainly improved the quality of the paper. The calculations with code FD were performed on the CRAY J916/6-1024 supercomputer of the University of Konstanz, Germany, and the calculations with code TREESPH were made on the CRAY YMP-4/432 supercomputer of the Universidad Nacional Autónoma de México. This work was supported in part by the Ministero dell'Università e della Ricerca Scientifica e Tecnologica of Italy and by the Consejo Nacional de Ciencia y Tecnología (CONACYT) of Mexico. One of us (JK) wishes to thank the International Centre for Theoretical Physics (ICTP), Trieste, Italy, and the Bundesministerium für Bildung und Forschung (BmBT) of Germany for partial support.

References

Barnes, J., Hut, P., 1986, Nat, 324, 446
Bate, M. R., Bonnell, I. A., Price, N. M., 1995, MNRAS, 277, 362
Bodenheimer, P., Boss, A. P., 1981, MNRAS, 197, 477
Boss, A. P., Bodenheimer, P., 1979, ApJ, 234, 289
Boss, A. P., Myhill, E. A., 1992, ApJS, 83, 311
Burkert, A., Bodenheimer, P., 1993, MNRAS, 264, 798
de Felice, F., Sigalotti, L. Di G., 1992, ApJ, 389, 386
Finn, L. S., Hawley, J. F., 1989, (unpublished report)
Gingold, R. A., Monaghan, J. J., 1977, MNRAS, 181, 375
Gingold, R. A., Monaghan, J. J., 1981, MNRAS, 197, 461
Hernquist, L., 1987, ApJS, 64, 715
Hernquist, L., 1993, ApJ, 404, 717
Hernquist, L., Katz, N., 1989, ApJS, 70, 419
Klapp, J., 1996, (in preparation)
Lucy, L., 1977, AJ, 82, 1013
Monaghan, J. J., Lattanzio, J. C., 1985, A&A, 149, 135
Monaghan, J. J., Lattanzio, J. C., 1986, A&A, 158, 207
Mönchmeyer, R., Müller, E., 1989, A&A, 217, 351
Myhill, E. A., Boss, A. P., 1993, ApJS, 89, 345
Nelson, R. P., Papaloizou, J. C. B., 1993, MNRAS, 265, 905
Nelson, R. P., Papaloizou, J. C. B., 1994, MNRAS, 270, 1
Norman, M. L., Wilson, J. R., Barton, R. T., 1980, ApJ, 239, 968
Sigalotti, L. Di G., 1993, Rendiconti del Seminario Matematico dell'Università e del Politecnico di Torino, Vol. 51, 3, 267
Sigalotti, L. Di G., 1996, (in preparation)
Steinmetz, M., Müller, E., 1993, A&A, 268, 391
Tscharnuter, W. M., Winkler, K.-H., 1979, Comp. Phys. Comm., 18, 171
van Leer, B., 1977, J. Comp. Phys., 23, 263

This article was processed by the author using Springer-Verlag LaTeX A&A style file *L-AA* version 3.